THE INFLUENCE OF REACTOR OPERATIONS ON THE DESIGN AND PERFORMANCE OF TOKAMAKS WITH SOLID-BREEDER BLANKETS

N. M. Ghoniem, M. A. Firestone and R. W. Conn
Mechanical, Aerospace and Nuclear Engineering Department
University of California, Los Angeles
Los Angeles, California 90024
(213) 825-4866

ABSTRACT

Operational aspects of a model tokamak system with a solid-breeder blanket are presented. The model blanket is an evolution of the STARFIRE and BCSS design studies. Full-power reactor operation is at a neutron wall loading of 5 MW/m^2 and a surface heat flux of 1 MW/m^2. The blanket is a pressurized steel module with bare beryllium rods and low-activation HT-9-(9-C-) clad $LiAlO_2$ rods. The helium coolant pressure is 5 MPa, entering the module at 297°C and exiting at 550°C. The system power output is rated at 1000 MW(e). In this paper, we present our findings on various operational scenarios and their impact on system design. We first start with the salient aspects of operational physics. Time-dependent analyses of the blanket and balance of plant are then presented.

INTRODUCTION AND BACKGROUND

A fusion power station will be a complex machine made up of numerous subsystems and components. The physics and engineering aspects of these subsystems, together with their dynamic interaction, will pose various constraints on the transient operation of the power plant. The startup procedures, constrained in this fashion, should be devised such that transient operation does not result in any major degradation of the overall economics. This argument underlies the basic interaction of startup procedures and base-line design. Startup requirements should therefore be incorporated in the base-line design.

Startup constraints can be divided into three general categories. The first are those which are due to the design of plant components. These subsystems are generally constructed to operate most efficiently at full power. As such, the plant may encounter severe difficulties operating steadily at fractional power. For example, the turbines may not be operational below 20% of their rated design parameters. Careful base-line design of components reduces the scope of these constraints.

A second set of constraints arises due to the dynamic interaction of the plant's subsystems. Each system has its own response time and these times can vary greatly. Usually, the dynamic behavior of the reactor is dictated by the subsystem with the slowest response time. The fusion core has a relatively fast response time which is basically determined by the ion-ion collision time and the rate of slowing down of α-particles in the system. Typical plasma response times are in the range of 0.5 to 3 sec. The engineering components such as blanket and thermal conversion systems have relatively long response times (minutes to hours or days). The rate of change in power is then dictated by the response time of these components. The fusion core should be programed to follow this time path. Moreover, the time the reactor spends in each phase of the startup procedure is generally determined by the response time of the subsystems involved in that phase.

Finally, there are some systems which are solely needed for startup where special equipment is generally needed. Startup procedures should be chosen which require a minimum of special startup equipment. The auxiliary heating systems required for full power operation should be used as fully as possible during startup while the total input power for startup should also be minimized for economic reasons. If the input power is small enough, it can be tapped directly from the electric grid system, eliminating special startup power storage and supply systems. The operation of large-scale experimental machines and fusion power reactors is divided into five general phases which will be briefly discussed here. (See Ref. [1] for more detailed discussion.)

Phase 0: Initial commissioning. Initial commissioning occurs once the construction of the device is completed and tests of all components and subsystems are carried out to make the device ready for operation.

Phase I: Cold or hot shutdown phase. Two distinct shutdown phases are possible. Phase IA

(cold shutdown) is expected to occur infrequently and would require that the blanket and other power related components be completely shut down. Phase IB (hot shutdown) is where the power conversion components and their coolants are maintained at near-ready operation conditions of temperature and pressure but there is no plasma operation.

Phase II: Plasma initiation and standby power phase. The operational specification of all systems, particularly those critical to the operation of the plasma, are tested in the absence of plasma in a component testing and checkout phase. During the first startup, plasma technology systems are tested simultaneously with plasma initiation and operation. Plasma auxiliary heating systems are used to achieve plasma parameters approaching those of full power operation, albeit without the use of deuterium-tritium (D-T) fuel. In this case, hydrogen may be preferred as the primary working gas to preclude neutron production and induced radioactivity.

Upon completion of component testing, the fusion core is deemed operational. A plasma using deuterium or deuterium and tritium can now be initiated and heated to fusion temperature, bringing the reactor to a standby condition. In the standby condition, the plasma produces thermal and fusion power between 1% and 20% of the rated power. In a reactor, the thermal power conversion system is unlikely to be operational during this phase so that no electricity can be produced by the thermal cycle.

Phase III: Staged or fractional power operation. The fusion system operates at fractions of full power while system tests are performed and licensing requirements are fulfilled.

Phase IV: Rated power operation. The fusion system power is produced continuously at its rated and licensed power level.

General constraints can be applied to the various startup phases. In order to minimize the startup equipment and input power, the plasma initiation phase should be implemented rapidly so the plasma can also be heated by fusion-born α-particles. On the other hand, the staged power increase phase to full power should be implemented slowly. This is due to the slow response time of the engineering subsystems.

The standby phase is especially important. The plasma is producing 1% to 20% of full power but the thermal conversion systems are not yet operational. Input power is needed to maintain the plasma in this phase. The plasma parameters in the standby phase should be carefully chosen to minimize this input power.

In the next section, we describe the main characteristics of a recent solid-breeder tokamak design by the UCLA group.[2-8] Then, results of plasma-burn dynamics and time-dependent electromagnetic modeling as it pertains to the various startup phases are discussed. Engineering analyses of critical subsystem responses and interactions follow. Finally, conclusions are presented.

A REFERENCE SOLID-BREEDER TOKAMAK FUSION SYSTEM

A reference blanket design for this startup study is a helium-cooled solid-breeder concept. The breeder material is lithium aluminate ($LiAlO_2$) which is in the form of metal-clad rods. The cladding material is 9-C, a low activation ferritic steel similar to HT-9.[9] A neutron multiplier zone of bare beryllium rods is included to enhance the tritium breeding. The blanket is divided toroidally into 24 sectors, each comprising 45 modules. While the sector configuration is that of a BCSS design,[10] individual modules have recently been designed at UCLA.[2-8] Figure 1 shows the configuration of a single module with neutron multiplier and breeder pins in three separate zones.

The coolant flows through the module shell and first wall (FW) and then enters the blanket. It then cools the neutron multiplier zone, followed by the tritium breeding zones. (Note that the breeding section is divided into two zones.) The larger rods, toward the back of the blanket, are sized to operate at a maximum centerline temperature of 1100°C for the $LiAlO_2$ pellets. Selection of pin sizes, geometry, and operating conditions is based on several design iterations involving neutronics, thermal analysis, structural analysis, and tritium inventory calculations. Table I summarizes the major operating parameters of the blanket design. While a more detailed description of this design can be found in Refs. [2-8], a list of its salient features follows.

(1) A pressurized modular configuration is used to allow for good use of space in tight-fitting locations.

(2) Helium coolant flow is mainly in the radial direction, helping to achieve a thermally homogeneous blanket.[3]

(3) Helium cross flow, combined with small pin sizes, results in minimal temperature asymmetries around the circumference of individual pins. This is shown to result in minimal bowing and deflections within the blanket.[6]

(4) Material allocations within the blanket are based upon neutronic optimization studies. The final blanket configuration shown in Fig. 1 is quite small, with total depth of 46.3 cm, including the manifolds and FW zones. Since the solid-breeder zone is only 21.8 cm deep, the amount of breeder material is small. The final breeding ratio (1-D) is calculated as 1.18.

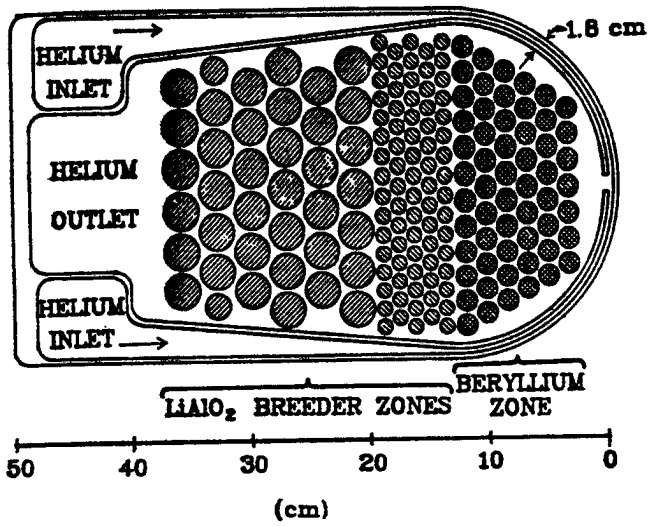

Fig. 1. Single module configuration for the reference solid-breeder blanket.

TABLE I. Major System and Blanket Parameters

Reactor type	Continuous burn D-T tokamak with He-cooled solid $LiAlO_2$ blanket
Major radius	5.7 m
Minor radius	1.56 m
Elongation	1.6
No. toroidal sectors	24
No. blanket modules/sector	45 (full poloidal coverage)
Blanket module type	He-cooled, pressurized module of 9-C structure (low activation martensitic steel)
Module poloidal height	0.28 m
Module mean toroidal length	1.50 m
Fusion power	2850 MW
Thermal power	3463 MW
FW 14 MeV neutron flux	5 MW/m^2
FW surface heat flux	1 MW/m^2
Coolant pressure	5 MPa
Coolent inlet temp	250°C
Coolent outlet temp	550°C
Coolant mass flow rate	2.21 × 10^3 kg/s
Thermal efficiency, gross	35%
Electric output, gross	1034 MW

PLASMA STARTUP, BURN ANALYSIS, AND OPERATION AT VARIOUS LEVELS OF OUTPUT POWER

The purpose of this part of the study is to develop the tools necessary to examine the transient behavior of tokamak reactors. To evaluate the physics performance during operation, the INTOR[11] design is chosen to perform a time-dependent system study. However, several plasma specifications have been altered to be consistent with recent experimental observations. The plasma edge safety factor, q_I, is 2.1 while the burn average toroidal β is 3.4%, agreeing with the Troyon limit.[12] The energy confinement time, assuming an L-mode scaling of $\tau_E = 0.3 I_p(MA)a^2(m)$, is 2.9 s. The average ion temperature remains at 10 keV and $n\tau_E$ becomes 3.66 x 10^{20} s/m^3, which means the plasma is ignited. Table II indicates the original INTOR parameters along with those chosen for this study.

Since the study of startup and staged power operation is aimed at identifying key issues for power reactors, we have altered the discharge scenario to allow for lower-hybrid RF current-drive ramp-up and OH current maintenance. This "hybrid" mode of plasma current maintenance allows for fractional-power and long-pulse (>1000 s) operation.

TABLE II. Plasma Parameters for This Study and the Original INTOR Values

	INTOR	UCLA/INTOR
Plasma major radius, m	5.3	5.3
Plasma minor radius, m	1.2	1.2
Plasma elongation	1.6	1.6
Plasma triangularity	0.2	0.2
Burn avg beta, %	5.6	3.4
Poloidal beta	2.6	1.6
Avg ion temp, keV	10.0	10.0
Avg ion density, m^{-3}	1.4×10^{20}	1.28×10^{20}
Energy confinement time, s	1.4	2.9
Plasma current, MA	6.4	6.4
Field on chamber axis, T	5.5	5.5
Safety factor at edge	2.1	2.1
Thermonuclear power, MW_{th}	620	510

Model for Reactor Electromagnetic Response

The plasma's changing electromagnetic environment is a key to the time-dependent system behavior affecting plasma equilibrium, stability, and energy confinement time. To this end we have modified a TFTR time-dependent electromagnetic and power balance code, PCIC,[13] to incorporate plasma shape, eddy current models, α-particle heating, and lower-hybrid current drive.

The calculation of gross plasma equilibrium parameters is necessary in a dynamic system description in order to determine the effects of changes in the electromagnetic environment in the plasma. Normally this is done using a free-boundary MHD calculation. We have developed a computationally fast method for determining plasma shape parameters from magnetic multipoles

of the external magentic field produced by the poloidal field coils and eddy currents.[14] These constitute a system of electric circuits which are solved together with the plasma and its power balance. Figure 2 shows a comparison of the free-boundary MHD results together with the plasma shape and position generated by the approximate multipole method. The agreement is quite satisfactory.

The plasma radial and vertical motion is determined from force balance, ignoring plasma mass. We include the time rate of change of the circuit currents and plasma parameters, in addition to the coupled radial and vertical motion.

We assume the vacuum vessel and blanket/shield[15] are infinitesimally thin toroidal sheets located at the center of the volume. The actual thickness and resistivity is incorporated into the resistance calculation. In Fig. 3 we have used three sheets to simulate the vessel, blanket, and shield. The sheets are broken into toroidal strips corresponding to individual eddy current circuits. The concentric sheet model simulates the poloidal field diffusion through a thick inhomogeneous structure. As an example, the strips are toroidally continuous, but resistive breaks could be incorporated.[16] INTOR has both divertor and pump limiter designs. For our example, we have

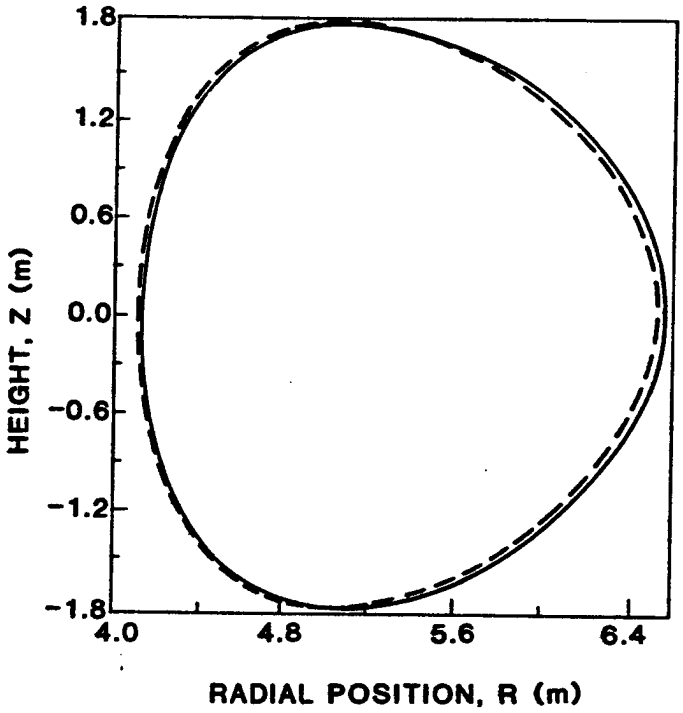

Fig. 2. Comparison of the multipole method for gross plasma equilibrium and actual free boundary MHD results for a 1.5 elongation and 0.2 triangularity plasma. This is for the INTOR tokamak. (Solid=exact; dashed=multipole).

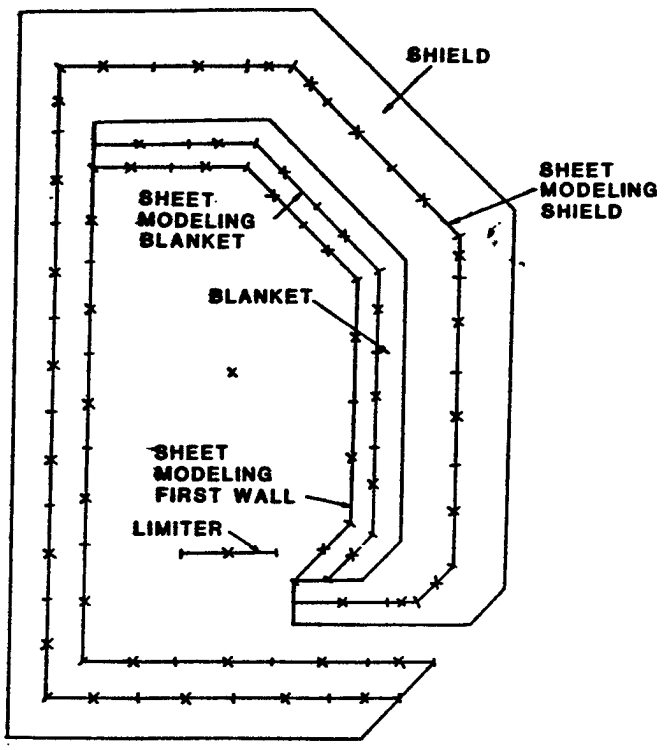

Fig. 3. Illustration of the "sheet" eddy current model for INTOR.

chosen the design with the limiter at the bottom.[17] The pump limiters and other external structures are modeled as conducting strips in the appropriate locations. The strips are mutually coupled to each other, the plasma, and the active field coils. These currents contribute to the poloidal field at the plasma and hence influence its equilibrium properties.

To determine the evolution of the RF-driven current profile, a ray-tracing code[18] is used which essentially follows the wave energy path, absorption, and current generation, given an incident lower-hybrid wave spectrum. For simplicity, a cold plasma wave description is used, the damping is assumed quasi-linear, and the current driven is obtained from the Fisch-Karney formula[19] for the normalized efficiency J/P. The resultant "steady-state" current profile can then be treated as a distributed current source over the entire plasma circuit. It should be pointed out that in this treatment, the effect of runaway electrons is neglected.

In a separate current ramp-up study, the ray-tracing code is coupled to WHIST,[20] a time-dependent, 1-1/2-D transport/equilibrium code developed at Oak Ridge. The current profile evolution is governed by a poloidal field diffusion equation, with the steady-state RF current profile acting as sources in each flux tube. Simple current ramp-up scenarios[18] for

INTOR at low densities were examined, with tearing mode instabilities invoked to model effectively inward current diffusion. A constant RF pulse of 10 MW was applied at a plasma density of $\langle n \rangle = 5\times10^{12}$ cm^{-3} and temperature $\langle \tau \rangle = 1.5$ keV, assuming a pre-formed current of 0.5 MA. For a plasma pulse of 300 s, the current rose to 4.4 MA, with an average L/R time of 60 s, and the ramp-up efficiency $LI(dI/dT)/P_{rf}$ starting at 5% and dropping to 3% towards the end of the pulse. A scenario involving current overdrive to shorten the ramp-up time and minimize energy input was also studied.

Tokamak Plasma Operation at Fractions of Rated Power

A commercial fusion reactor must be able to operate at fractions of full power and to maintain thermal stability. We have used steady-state[21] and time-dependent[22] 0-D plasma-burn codes and determined that active feedback of ion fueling and auxiliary power is required to control power and maintain thermal stability. This is true even in the most strongly stable regions, i.e., at low plasma density and high plasma temperature, where reactor net power output is low. Burn control is found to be easiest if there is a soft β-limit, wherein the transport losses increase without plasma disruptions as β approaches the Troyon limit.[12] In this case the ignition region is accessible and operation is stable up to the Murakami density limit. A hard β-limit would require confinement degradation to operate at high output power.

Fractional power operation can be achieved by varying the ion fuel ratio, changing the plasma current, or altering confinement[23] from H-mode to L-mode, if the reactor has a divertor. The strategies for burn control and fractional power operation vary according to the assumed energy confinement scaling. Optimistic scaling laws with respect to ignition pose the greatest problems for burn control because their operating region is well above the ignition curve in the thermally unstable region. An example of such a τ_E scaling law is neo-Alcator scaling. Additionally we find that neoclassical ion transport leads to very optimistic ignition criteria when compared to anomalous ion loss for the global transport losses.

It is found experimentally that auxiliary heating of tokamak plasmas causes a degradation in confinement. This so-called L-mode scaling has been analyzed parametrically by Kaye and Goldston.[23] A major open question is whether alpha heating will also cause confinement degradation. Also, operation with a divertor has led to the so-called H-mode in which the confinement time can be twice the value in the L-mode regime. We have therefore thoroughly examined whether and how tokamak reactors can be operated, depending on scaling law and physics regime.

We find thermally stable ignited tokamak operation for the following cases:

(1) When the plasma is marginally ignited with the ion fuel source and auxiliary power synchronized to an active feedback system;

(2) When the plasma has a soft β-limit;

(3) When the scaling law is such that only a small fraction of α-particle power degrades confinement (if full degradation occurs, an INTOR-size tokamak will not ignite);

(4) When auxiliary power degrades confinement but the region well above ignition is accessible and stable with auxiliary power feedback;

(5) When plasma confinement degrades with temperature instead of power;

(6) When plasma confinement shows a saturated power scaling, such as $\tau_E \sim (a + b/P)$, rather than the Kaye-Goldston scaling, $\tau_E \sim P^{-1/2}$. Here, P is the non-ohmic heating power.

Maintaining thermal equilibrium while varying the output power requires marginally ignited operation attained by moving along the ignition curve in n-T space. A number of mechanisms are available for changing the ignition point, depending upon the assumed energy confinement scaling. Primarily we have examined variations of plasma current, density, fuel mixture ratio, auxiliary power, and plasma size and/or shape.

The connection between the electromagnetics and a burning plasma can best be seen from the following three equations for the energy confinement time, safety factor, and critical β-limit:

$$\tau_E \propto f(R,a,\mu)I_p \quad , \tag{1}$$

$$q_I = \frac{5\, B_o(T)a^2(m)}{R(m)I_p(MA)}\left(\frac{1+\kappa^2}{2}\right) \quad , \tag{2}$$

$$\beta_c = C(\kappa,\delta,i)\,\frac{I_p(MA)}{a(m)B_o(T)} \quad . \tag{3}$$

The energy confinement time and critical β-limit are proportional to plasma current. The edge safety factor, energy confinement, and β-limit depend upon plasma size and shape. Since the electromagnetic environment is responsible for plasma current, size, and shape, it therefore influences the burning plasma energetics. As discussed, the assumed τ_E scaling and β-limit influence how burn control and fractional power operation are accomplished.

As an example of the interrelationships, consider moving between two output power levels, 1000 MW and 500 MW, in the density-temperature plot of Fig. 4., assuming modified Kaye-Goldston scaling. For simplicity, let us assume there exists a soft β-limit and that the power is changed by modifying either density or temperature, but not both. This case is illustrated in the figure as moving from point A to point B.

Reduction of power from 1000 to 500 MW. Starting at point A in Fig. 4, we wish to reduce the power from 1000 to 500 MW. Since the most efficient reactor operation is at the β-limit, β_c, one should aim to decrease β_c such that its curve crosses the 500 MW curve near the desired operating point. If the power reduction is to be achieved by decreasing the density at constant temperature (A → B), the plasma triangularity should be decreased along with the density. If β_c had been lowered by decreasing I_p, τ_E would be proportionally lowered [Eqs. (1) and (3)] resulting in a temperature decrease. Reducing the power at constant density (A → C), requires a spoiling of confinement to lower the plasma temperature. Here the logical method is to reduce the plasma current, thereby reducing confinement and β_c together.

Increase of power from 500 to 1000 MW. If the power is to be increased by changing density (B → A), the plasma triangularity should be increased such that β_c crosses the 1000 MW curve at point A. If the plasma current were increased, <T> would increase because of the enhanced confinement. A more serious objection is that q_I might fall below the limit required for stability or for soft β-limited operation.[24] An increase in power with temperature (C → A) can most easily be performed by increasing plasma current. This naturally increases both temperature through enhanced confinement and β_c. Again, there could be problems if q_I decreases. In that case, a combination of increases in plasma current and elongation should maintain q_I while increasing <T> and β_c.

These two examples are oversimplified but useful for illustration. The confinement time and critical β-limit are not linear functions of shape. Also, the interplay between confinement time and temperature is more complex than assumed above. In reality, an appropriate path may include both density and temperature changes (e.g., A → D or D → A in Fig. 4). By assuming a soft β-limit, the question of active burn control has been ignored. Experimentally, most evidence to date indicates the β-limit is hard and that active burn control will be required to avoid disruptions in tokamaks. Burn control can be considered as very small changes around a nominal power level, and therefore the same techniques described above could be applied. Finally, if the confinement time is inversely proportional to the square root of the auxiliary power (Kaye-Goldston scaling), the auxiliary power could be used for burn control or power changes. Since the aim is to operate near the β-limit, changes in plasma current, size, or shape would still be required in conjunction with auxiliary power modification.

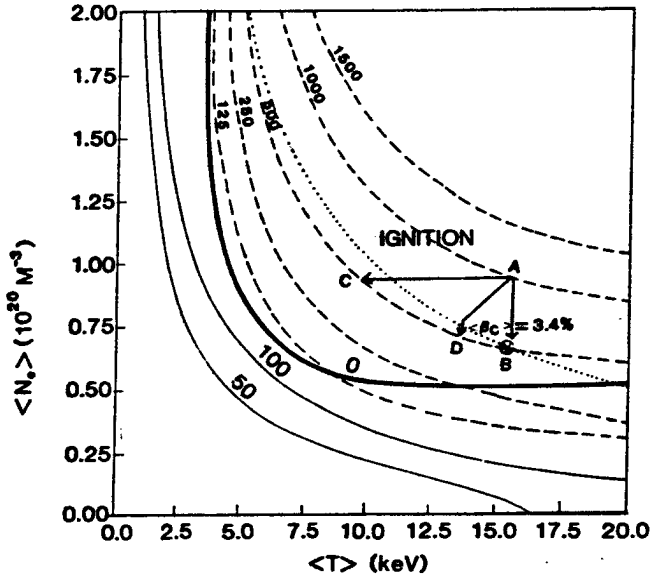

Fig. 4. Fusion power and critical beta Goldston scaling without alpha degradation.

These results tempt comparison with an earlier study of tandem mirror reactors, START(TM).[1] The primary finding was that if radial transport is negligible, the input power can be simply controlled by varying the center cell volume. This is accomplished by controlling the magnetic field at the direct converter. Additionally, the direct converter allows zero net power operation even for small fusion power. The tokamak reactor, on the other hand, allows no straightforward technique for power modification. First, both the design and operation of the tokamak depend upon its assumed energy confinement scaling. For example, if it is required to operate well above ignition for useful net power, the reactor has been overbuilt. Second, the actual techniques for burn control and power modification depend strongly on the assumed scaling. Finally, the coupling between the energy confinement time and the MHD quantities, q_I and β_c, [Eqs. (1)-(3)], further complicate burn control and power modification. The operations which depend upon energy confinement changes must not adversely affect plasma equilibrium and stability. These issues all make burn control and fractional power operation in a tokamak a much more significant and difficult problem.

ENGINEERING STARTUP ANALYSIS

A serious concern relating to fractional power operation is the time rate-of-change from one power plateau to the next. The time rate of power production, which is controlled by plasma collisional and transport mechanisms, is quite fast and on the order of few seconds, as shown earlier. If the power loading on the FW and blanket are increased on this time scale, severe transient thermal fields could develop. These transients result from the coolant-flow response time in the primary loop. The coolant-flow time constants can range from 10s to 100s of sec. The longest time constant is the time required

to reach thermal equilibrium after a change in the level of power production. We will first discuss the thermal response of the blanket during power variations. This is followed by a thermo-mechanical analysis of the solid-breeder blanket during various operational scenarios. Finally, tritium transport is modeled to prescribe operational procedures that lead to minimum tritium inventory.

Transient Thermal-Hydraulic Analysis

Using the time-dependent option of the finite-element code (TACO-2D),[25] a range of power ramp conditions was investigated and the temperature histories for the FW structure were analyzed. Both power ramp and coolant flow rates were varied during these studies. The power in each case started at the 50% level and was ramped up to full power. The entire ramping cycle lasts from 5 sec to 50 min, depending on the specific case.

Calculation results are shown in Fig. 5. Case A is for a fast power increase rate (10%/sec) and a slow flow increase rate (1%/min). Case B is for a fast power increase rate (10%/sec) and a moderate flow increase rate (10%/min). Case C is for a fast power increase rate (10%/sec) and a fast flow increase rate (10%/sec). Finally, Case D is for a moderate power increase rate (10%/min) and a fast flow increase rate (10%/sec). The most severe conditions exist when the change in coolant flow rate is slower than the change in power production (Case A). The FW structure reaches a maximum temperature of 702°C and then slowly cools down. It is desirable to ramp power and coolant flow at the same rate, or even to increase the coolant flow rate faster than the rate of power increase. Plasma power ramp rate will therefore be dictated by the available flow ramp rate. Much slower flow and power ramp rates must be used during initial startup.

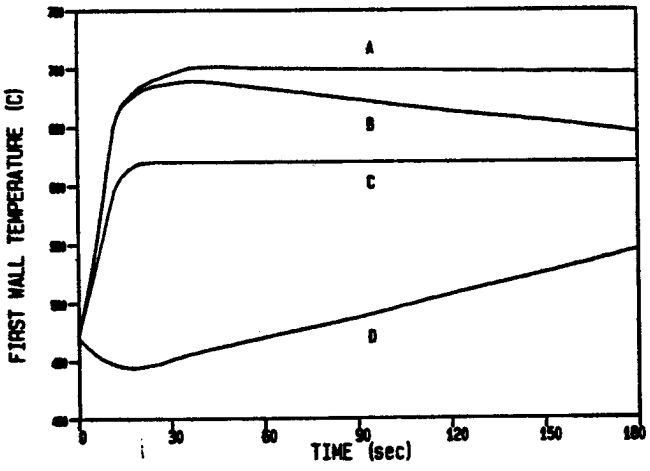

Fig. 5. Thermal response of the FW surface temperature under various power and coolant flow ramps. (A) Power = 10% s^{-1}; flow = 1% min^{-1}; (B) Power = 10% s^{-1}, flow = 10% min^{-1}; (C) Power = 10% s^{-1}, flow = 10% s^{-1}; (D) Power = 10% min^{-1}, flow = 10% s^{-1}.

The time constant for the FW structure is generally on the order of 10s of sec and is quite dependent on the power ramp rate/flow ramp rate ratio. However, the multilayer breeder pins respond to thermal transients on a longer time scale because of their inherently slow thermal diffusivity. The breeder rods studied were the first row of 3-cm-diam pins (row 6). These pins were chosen because they have a longer themal time constant as compared with pins in rows 1-5. The ramp rate for both power and flow was chosen as 10%/min. The time response of the centerline temperature closely follows the power ramp and reaches equilibrium at 600 sec. It is interesting to note that the inherently slow thermal response characteristics of breeder pins determines the overall heat transfer rate from inside the pins. It is concluded therefore that flow rate control is extremely important to the reduction of first wall thermal transients. The breeder material has an inherent capacity to reduce temperature fluctuations resulting from rapid power increase rates.

The situation described above is more applicable to rapid power variations during hot startups. As will be shown later, however, the initial startup of the fusion system requires much slower rates of power variations. Because of the development of high stresses between the cladding and solid breeder material, a matched power and flow ramp rate of ≈1%/hr is to be used.

An important consideration of thermal transient analysis is the ability to determine the necessary requirements and procedures for the primary loop preheat. It is desirable from the viewpoint of reactor operations to perform hot functional tests prior to power generation. This ensures the functionality of components under operating temperatures and pressures. To perform hot functional testing, the primary loop must be heated with an auxiliary heat source. It has been previously shown[1] that helium gas preheat is more desirable than other gas systems.

Taghavi and Ghoniem[26] developed a model for fusion reactor preheat analysis. The analysis presented here is an extension of their work to account for the physical differences in the specific reactor design. In a lumped capacitance model, the time constant for each component is estimated by

$$\tau_i = \left(\frac{\rho C_p V}{Ah}\right)_i , \qquad (4)$$

where ρ is the density, C_p is the heat capacity at constant pressure, V is the volume, A is an effective surface area, and h is an effective heat transfer coefficient. Various component time constants are given in Table III.

All of the primary loop components are initially at ambient temperatures (≈20°C). During the hot functional testing phase, we will operate all components at 250°C. We also assume here for simplicity that no major heat loss mechanisms take place during this phase. The energy required is simply calculated by summing up energy contributions required for all components to reach a temperature of 250°C. This is estimated to be ≈25 MW-hr.

We will assume that the heater can continually produce hot helium with an outlet temperature of 400°C. Figure 6 illustrates the temperature history of the primary loop components during preheat. It is seen that the first half of the primary piping heats up quite rapidly, reaching the desired temperature of 250°C in ~20 min. It is suggested though that the primary loop be heated in reverse order to normal coolant circulation. Thus, the hot leg of the primary piping is heated up first, then the blanket, and finally the cold leg of the primary. Now the hot leg, which normally operates at 550°C, will be at 400°C for the majority of the preheat cycle. The average thermal power required for this cycle is estimated to be 8.4 MW.

TABLE III. Time Constants for Various System Components

Component, i	t_i (s)	Total No. Components with τ_i
1/2 primary piping	750	2
FW plus module shell	57	1,080
Be rods	24	64,800
$LiAlO_2$ rods		
1.22 cm o.d.	45	86,400
3.0 cm o.d.	150	45,360

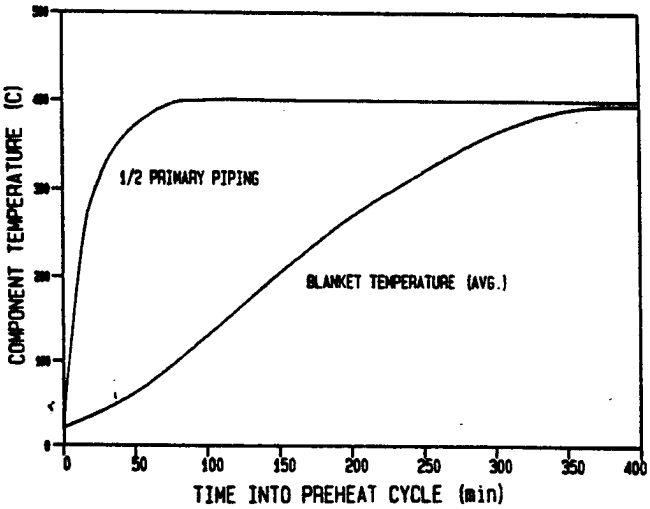

Fig. 6. Temperature histories for various primary loop components during the pre-heating phase.

Breeder-Cladding Mechanical Interaction

Finding the smallest allowable ramp rate for startup is important for the economy of the operation, since overly conservative startup can amount to substantial percentage of the power cycle. In the stage of preliminary design the main concern is failure of the cladding due to high stresses or large total strains. The following analysis provides a simplified tool for design based on macroscopic mechanical interaction between the breeder and the cladding.

Since the thermal field[3] exhibits only a slight azimuthal asymmetry, the problem is formulated based on an axisymmetric analytical solution for the radial temperature distribution. Interaction between the changing geometry and the thermal field has been neglected during the course of the analysis. The size of the developed gap is on the order of hundredth of a millimeter, which justifies this simplification.

Material models for the breeder pellet include linear elastic behavior, linear thermal expansion, and temperature-dependent swelling. The cladding material was assumed to exhibit linear elastic behavior, linear thermal expansion, and temperature-dependent creep. All linear material properties are taken as constants, although temperature dependence, especially in the breeder pellet, may have an influence on the results. The details of the thermostructural breeder pellet clad interaction model are given in Ref. [4].

To simulate real operational conditions, a typical time history is used. One cycle consists of a power ramp, operation at full power, shutdown, and radiation swelling time at preheat temperature. If creep deformation occurs during the cycle, then there will be a residual plastic strain in the clad after it separates from the breeder pellet. This effect is equivalent to a permanent increase in the clad diameter and causes it to reach contact with the breeder pellet in the subsequent startup at a later time within the cycle.

Following are the effects of several important variables on the pellet-cladding mechanical interaction problem.

Solid breeder/cladding compatibility. The stresses for different designs under the same thermal operating conditions are shown in Fig. 7 for $LiAlO_2$ and 9-C cladding. Solid lines represent the thermoelastic stresses had plastic

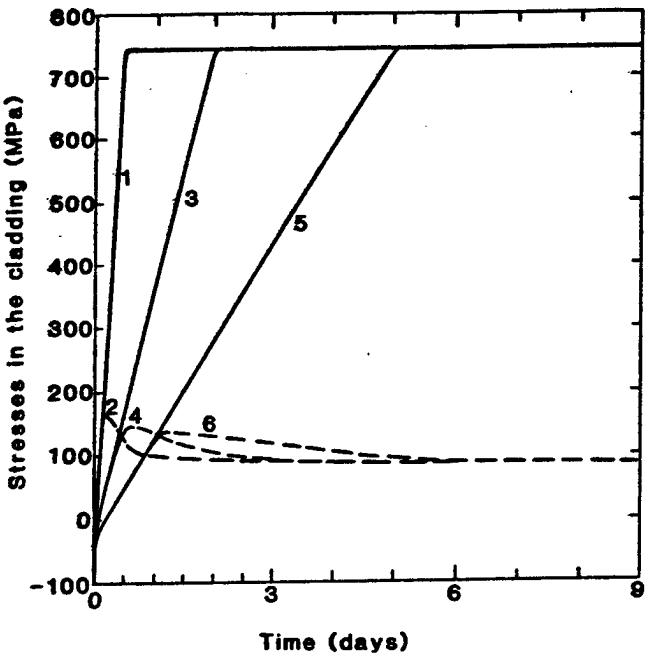

Fig. 7. Cladding stress evolution for the first row of pins (Zone 2). No initial gap is assumed and the pre-heating temperature is 550°C.
1 = elastic (0.5 days to full power),
3 = elastic (2 days to full power), 5 = elastic (5 days to full power); 2, 4, and 6 = inelastic.

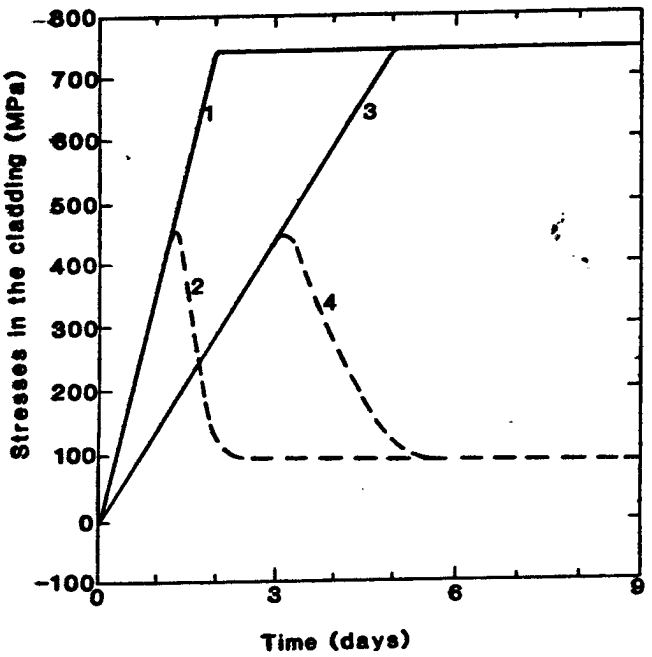

Fig. 8. Cladding stress histories for the first row (Zone 2), with zero initial gap. No pre-heating is assumed. 1 = elastic (2 days to full power), 3 = elastic (5 days to full power); 2 and 4 = inelastic.

strains not developed; broken lines correspond to the modeled interaction. Swelling of the breeder pellet has been neglected for these runs. Since the coefficients of thermal expansion for the solid breeder is close to that of the cladding, displacement of the pellet surface and the cladding is nearly matched. Consequently, the same elastic stress levels occur at significantly smaller gap sizes—an advantage for thermohydraulics and operational purposes. In fact, zero initial gap is safe for this design as will be shown in the integrated analysis.

Preheating. Figure 8 shows the results for the same material choice, steady-state temperature profile, and geometry as Fig. 7. This time, the system is not preheated to 550°C. Because the coefficient of the thermal expansion for the cladding is slightly higher than that for the pellet, there is no initial contact when the pin is preheated. Compressive stress because of coolant pressure develops in the cladding. Its value is about one third of the critical buckling stress which represents adequate margin of safety. From a structural point of view, the advantage of preheating is the interaction occurring at cladding temperature which permits creep. Therefore during startup, stress relaxation can significantly relieve peak stress.

Temperature ramp. Figures 7 and 8 illustrate the sensitivity of the results to the temperature ramp rate. When the slope of the temperature ramp is low, the cladding can creep more before steady-state profile is attained. The resulting displacement helps to accommodate the thermal expansion of the pellet. A power ramp rate of 20%/day will not result in excessive peak stresses.

Breeder pellet swelling: integrated analysis. Figure 9 shows the interaction under cyclic operation when swelling of the breeder pellet is included. Swelling gradually builds up and, instead of the decreasing stresses, a slight increase and eventually higher stress levels occur. Accumulated plastic strain also limits breeder pin lifetime. The figure depicts the plastic strain histories over four cycles for the $LiAlO_2$/9-C design. Reflecting the stress relaxation process, elastic strains decrease while plastic strains increase. The plastic strains stay below 0.5%. The same stress and strain components are shown for the Li_2O/2.25Cr-1Mo design over one period. In this case, swelling of the breeder pellet is stronger but the creep rate is also higher so stresses remain low. On the other hand, the accumulated plastic strain exceeds the 1% value by the end of the first power cycle, which indicates failure of the breeder pin. Because of this last finding and the sensitivity of the peak stress to the gap size, the $LiAlO_2$ design is recommended. It is also found that the peak stress occurs only during the first cycle. In subsequent startup cycles, contact between the pellet and cladding is delayed, and the developing stress is almost totally relaxed to the

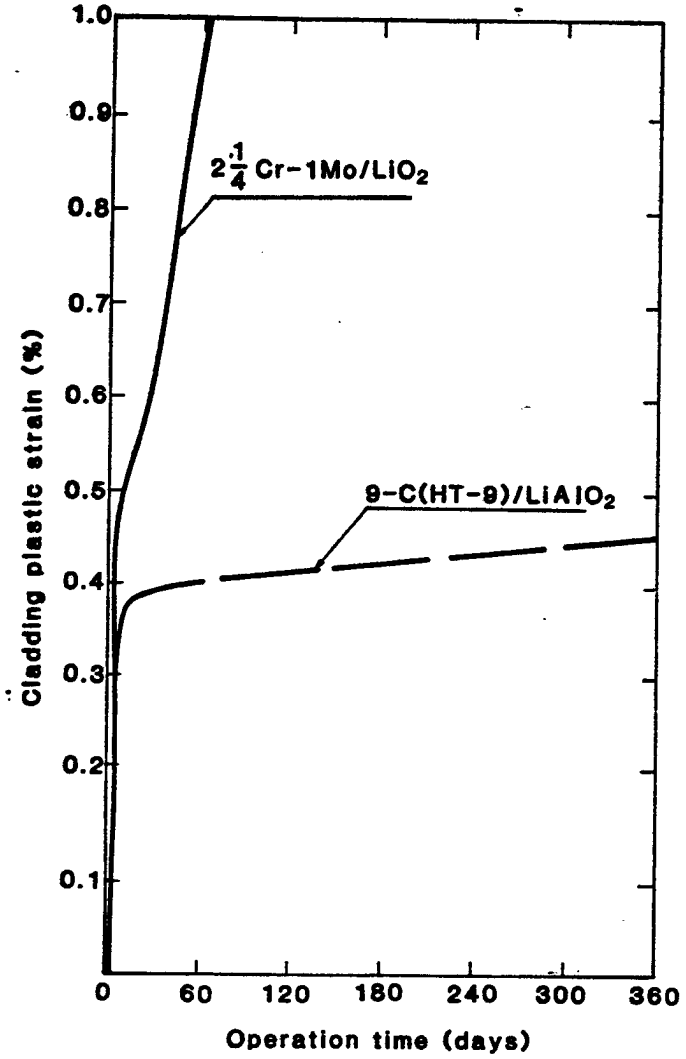

Fig 9. Accumulated cladding plastic strain during operational cycles for 9-C(HT-9)/$LiAlO_2$ and 2-1/4Cr-1Mo/LiO_2.

threshold creep stress. This means that subsequent hot startups can be much faster as discussed in the earlier section.

Blanket Tritium Analysis During Transients

Tritium inventory is controlled by diffusive and solubility properties. Tritium diffusion plays a major role in determining tritium inventory; the slower the diffusion, the longer the residence time within the blanket, and the greater the diffusive inventory. For $LiAlO_2$, there is a great variation in the experimentally determined diffusion coefficient.[27,28] The entire tritium inventory within the blanket solid breeder can be represented by:

$$I_b = I_d + I_s + I_a + I_g + I_p \quad ,$$

where I_d is the diffusive inventory, I_s is the inventory associated with solubility within the blanket, I_a is the adsorbed inventory, I_g is the grain boundary inventory, and I_p is the porosity/percolation/purge stream convection inventory. The total inventory, I_{tot}, is composed of I_b plus contributions from coolant contamination and metal structure permeation. Analysis of the order of magnitude of these inventory contributions and the available experimental data is given in Ref. [8]. For the $LiAlO_2$ use, the diffusive inventory is identified as the major contribution. The DIFFUSE[29] code is used to model tritium inventories during transients (see Ref. [8]).

Reactor startup was modeled for two different situations: (1) helium coolant flow at 100% of full power status and (2) significantly reduced helium flow during the transients to achieve higher operating temperatures and lower transient tritium inventories.

The transients modeled were at 10%, 20%, 50%, and 80% of full power, each lasting 3.5 days, followed by 100% power. The percentage of full power was used to scale the volumetric heating rates for ceramic and cladding accordingly, and likewise for tritium generation rate. The rise in coolant temperature from module entrance (constant at 250°C) to each row of pins was taken as a corresponding percentage of the temperature rise at full power.

The diffusive inventory was obtained from the DIFFUSE output at any point during the two weeks prior to full power. After two weeks, the input parameters were set at full power values and the inventory soon returned to its steady-state values. The total transient inventories were obtained as function of time for each row, and summed for the total blanket inventory.

The transient results involving 100% helium flow gave total blanket inventories of 226 g after 3.5 days at 10% power, 621 g after 3.5 days at 20% power, 429 g at 50% power, 61 g at 80%, and a short time at 100% returned the total inventory to the steady-state value of 12.6 g. These results are plotted in Fig. 10. The inventories are obviously much higher than steady-state during 10%, 20%, and 50% power levels, reaching several hundred grams with the largest contribution from the first row and its dominant tritium generation rate. The characteristic temperatures ranged from 277° to 317°C at 10% power, 317° to 377°C at 20%, 407° to 557°C at 50%, 507° to 737°C at 80%, and 567° to 857°C at full power. The temperatures fall within the regime of very slow tritium diffusion for 10% to 50% power, leading to rapid buildup of the bred tritium within the pins.

These significant inventories could lead to safety-related concerns of large blanket inventory, especially for protracted startup times at

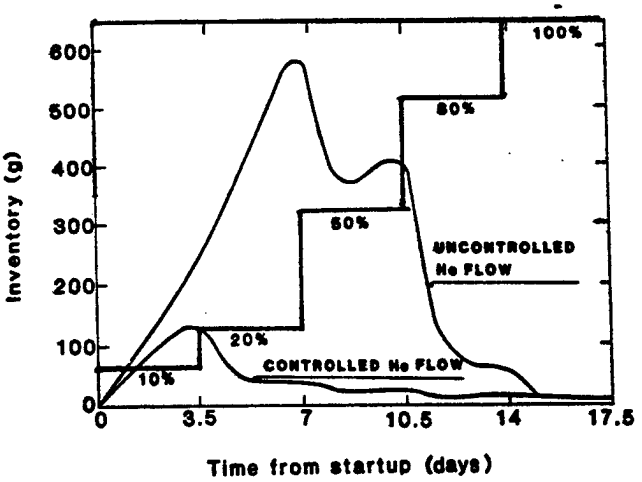

Fig. 10. Transient blanket tritium inventory for a typical startup scenario.

these temperatures. For this reason, the same startup regime was re-analyzed under conditions of restricted helium flow, reducing the rate of cooling and allowing higher temperatures to be achieved within the breeder. For the 10% and 20% power transients, the helium flow rate was set at 20% of that at full power. Thus, at 20% of full power the same coolant temperature should be obtained for each row as at 100% full power. Likewise, at 50% and 80% of full power the helium flow rate was set at 50% and 80% of full power, again giving the same coolant temperatures. For 10% of full power, with helium flow set at 20%, the rise in temperature between blanket inlet and the row in question was taken to be one half that at full power. The volumetric heating rate and tritium generation rate were scaled down from full power according to the transient power level as mentioned previously.

Because of considerably higher ceramic temperatures under these conditions of controlled coolant flow, the total blanket inventories were greatly reduced from the full power flow transients. The results give total inventories of 153 g at 10% after 3.5 days, 40.2 g at 20%, 25.6 g at 50%, and 16.5 g at 80%. These results are also shown in Fig. 10.

The results for these two cases clearly show the need for tailoring the helium flow rate to the transient power levels. An extended startup could lead to massive inventories if full power flow conditions are used. Even with controlled flow, a gradual inventory buildup might be a concern for low power levels over an extended period of testing. In this case, supplemental pre-heating of the coolant would alleviate such concerns. Further study of the minimum practical helium flow rates is also warranted: the minimum of 20% of full power flow is a conservative estimate, to avoid problems with flow instabilities.

For shutdown, two different cases were analyzed: (1) coolant flow at 20% of full power and (2) a combination of coolant flow reduction and heating such that the coolant temperature ranged from 470° to 500°C across the pins. This second scenario can be thought of as "baking" the blanket to speed its purging of tritium inventory. Both scenarios assume afterheat volumetric generation of 1% of full power and zero tritium generation.

For the first case, that of simply reducing the helium flow, the temperature of the coolant entering the blanket was again 250°C, and the temperature rise at each row of pins was taken to be 1/20 that of full power. These new coolant temperatures, 1% volumetric heating, and a corrected heat transfer coefficient were used to calculate new temperature profiles across the pins as before, and diffusion-averaged temperatures were again calculated for each pin. These temperatures were used as input to DIFFUSE along with zero generation rate as an additional step following the analysis for the three-year run at 100% power. Thus, the solid-breeder grains start with their steady-state inventories, then instantaneous shutdown occurs at which no more tritium is generated but the steady-state concentration profiles within each grain are now subjected to the much lower temperatures at shutdown. As can be expected, tritium diffusion from the grains slows down drastically. The diffusive inventories are modeled for a year after shutdown, with total blanket inventory calculated as before.

Figure 11 shows that, after two weeks, the total inventory is reduced from the steady-state full-power inventory of 12.6 g to 12.4 g, only a 1.6% decrease in total inventory. At the end of six months at these shutdown conditions, an inventory of 12.1 g still remains and after one year an inventory of 11.7 g, indicative of the almost negligible rate of diffusion at these cold shutdown temperatures. In comparison, the characteristic grains are then modeled for hot shutdown, with the coolant temperature of 500°C. As could be expected, the result was a significantly accelerated tritium purge from the blanket. Also Fig. 11 shows that, after two weeks, the inventory was reduced to an insignificant 0.02 g. Such auxiliary heating should alleviate inventory concerns in a post-shutdown environment.

SUMMARY AND CONCLUSIONS

Design and performance analysis of fusion power systems must take serious consideration of their operational characteristics. In this paper, a comprehensive assessment of the physics

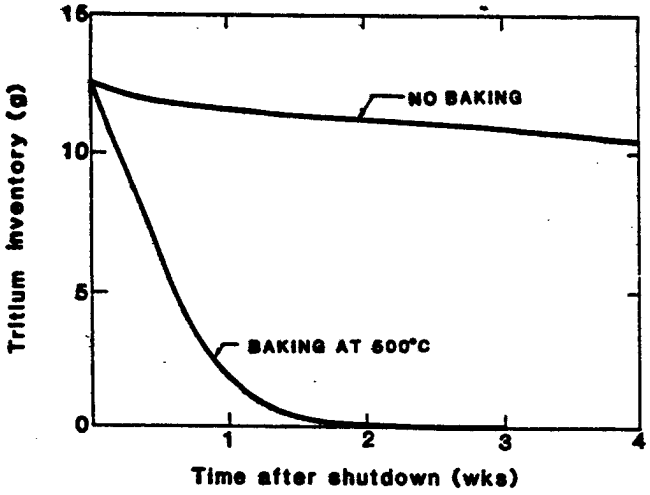

Fig. 11. Shutdown tritium inventories for a characteristic blanket temperature of 270°C and a bake-out temperature of 500°C.

and engineering operational design constraints is given for a model tokamak with a solid-breeder blanket. The following are conclusions of the study.

(1) Startup/shutdown operational design constraints are due to: (a) special component design requirements, (b) dynamic plant subsystem interactions, and (c) special startup components.

(2) Operation of fusion power systems can be divided into five phases: (a) initial commissioning, (b) cold or hot shutdown, (c) plasma initiation and standby power, (d) fractional power operation, and (e) rated power.

(3) The longest time scales are dictated by engineering constraints rather than physics performance. The rate of fusion power variation must be slow enough to meet the following limitations: (a) stress and material compatibility limitations (e.g., mechanical interaction between the breeder and structure system); (b) auxiliary power limitations; a total energy of 25 MW-hr is required to preheat the primary loop and blanket to 250°C; (c) mechanical limits; pump and valve inertia is responsible for the slow response of the primary coolant to rapid power variations.

(4) From simplified analysis, it is evident that the passive electromagnetic environment (eddy currents) could significantly affect the plasma equilibrium and control. This is the impetus behind our electromagnetic modeling described in this paper. We built our models (eddy current, plasma position and shape, lower hybrid current drive) such that they would all be consistent and could be brought together in a total systems code. This part of the effort is still in progress.

(5) Fractional power operation studies show a strong dependence on the energy confinement scaling assumed, both for reactor design and operation. Burn control and transitions between power levels are seen to be closely related with appropriate control levels including auxiliary power, fueling rate (density), and confinement control. This last knob ties back into the electromagnetic work since confinement is dependent upon such MHD quantities as plasma current, size, and shape. It is noted that changes in confinement must occur in a manner conducive to plasma stability and equilibrium. Finally, we demonstrated lower hybrid current ramp-up with our ray-tracing code coupled to a transport/equilibrium code.

(6) The time constants for the FW structure are generally on the order of 10s of s, while those for the solid breeder are on the order of 10s of min. The ramp rates must be matched for both power and flow, and slow enough (<10%/min) so as not to result in excessive FW transient temperature rise.

(7) The preheating energy required for the nominal 1000 MW(e) plant is on the order of 25 MW-hr. It is estimated that less than three hours are required to bring the system to its operating temperatures. The controlling factor is the response time of the blanket system.

(8) Mechanical interaction between the solid breeder and cladding materials is driven by intermittent system operation. A fast start-up results in high transient cladding peak stresses which eventually relax to the threshold stress for creep deformation. Prior preheating to 550°C for the $LiAlO_2$/9-C design allows thermal creep to mitigate the developing high stresses. An initial startup rate on the order of 1%/hr is recommended to avoid the development of high transient stresses.

(9) Cladding plastic strains accumulate during preheat cycles, but do not exceed 0.5% for one year of operation.

(10) Unrestricted coolant flow during startup ramping will lead to hundreds of grams of tritium inventory. Reduction of coolant flow can keep inventory at acceptable levels.

(11) Intermittent blanket preheating to 550°C during shutdown can lead to rapid purging of residual tritium.

ACKNOWLEDGMENTS

This work was supported by the U.S. Department of Energy, Office of Fusion Energy, Grant #DE-FG03-80ER52061, with UCLA. Thanks also to the UCLA design team of J. Blanchard, R. Martin, G. Orient, S. Grotz, S. Sharafat, T. K. Mau, C. Kessel, and E. Vold.

REFERENCES

1. "START/TM: A Study of Start-up and Fractional Power Operation of Tandem Mirror Fusion Reactors," R. W. CONN, N. M. GHONIEM and F. NAJMABADI, Eds., PPG-764, UCLA (NTIS, Springfield, VA, 1984).

2. P. LEVIN and N. M. GHONIEM, "Neutronic Optimization of a $LiAlO_2$ Solid Breeder Blanket," in Proc. this meeting, to be publ. Fusion Technol.; also ENG-8607/PPG-933, UCLA (1986).

3. S. P. GROTZ and N. M. GHONIEM, "Thermal Analysis of a Pin-Type Blanket for Tokamak Reactors," ibid.; also ENG-8612/PPG-938, UCLA (1986).

4. G. E. ORIENT and N. M. GHONIEM, "A Model for the Mechanical Interaction Between Solid Breeder and Cladding Materials," ibid.; also ENG-8610/PPG-936, UCLA (1986).

5. Ibid., "Elastic Structural Analysis of the Pin-Type Solid Breeder Blanket First Wall," ENG-8609/PPG-935, UCLA (1986).

6. J. P. BLANCHARD and N. M. GHONIEM, "The Bowing of Solid Breeder Rods in a Pin-type Fusion Blanket," in Proc. this meeting, to be publ. Fusion Technol.; also ENG-8605/PPG-931, UCLA (1986).

7. Ibid., "Thermomechanical Analysis of Solid Breeders in Sphere-Pac, Plate, and Pellet Configurations," ENG-8606/PPG-932, UCLA (1986).

8. R. MARTIN and N. M. GHONIEM "Modeling of Tritium Transport in a Fusion Reactor Pin-Type Solid Breeder Blanket Using the DIFFUSE Code," presented at ICFRM-2 (Chicago, March 1986), to be pub. J. Nucl. Mater.; also ENG-8608/PPG-934, UCLA (1986).

9. D. S. GELLES and M. L. HAMILTON, "Effects of Irradiation on Low Activation Ferritic Alloys," DOE/ER-0045/13, Dept. of Energy (Sept. 1984).

10. D. L. SMITH et al., "Blanket Comparison and Selection Study, Final Report," ANL/FPP-84-1, Argonne Natl. Lab. (Sept. 1984).

11. W. M. STACEY, Jr. et al., "U.S. INTOR, the U.S. Contribution to the International Tokamak Reactor Phase-I Workshop," USA INTOR/81-1 (1981).

12. F. TROYON et al., Plasma Phys. and Cont. Fusion, 26, 209 (1984).

13. R. J. HAWRYLUK, M. A. FIRESTONE, U. R. CHRISTENSEN, H. FISHMAN and J. A. SCHMIDT, "Plasma-Circuit Interaction in TFTR," TFTR Physics Group Report 29, Princeton Plasma Physics Lab. (1980).

14. C. E. KESSEL and M. A. FIRESTONE, "Determination of Gross Plasma Equilibrium from Magnetic Multipoles," in Proc. this meeting.

15. M. A. FIRESTONE, D. I. BROWN, C. KESSEL and M. TILLACK, "Eddy Current Models for a Tokamak Reactor Vessel and Blanket/Shield," in Proc. 11th Symp. Fusion Eng., Austin, TX, 1985.

16. D. I. BROWN, M. G. BELL and J. COONROD, Proc. 10th Symp. Fusion Eng., IEEE 83CH1916-6-NPS, p. 1233, IEEE (1983).

17. U.S. FED-INTOR and U.S. Contribution to the INTOR Phase-2A Workshop, USA FED-INTOR/82-1 (1982).

18. T. K. MAU, M. R. ILGEN and R. W. CONN, "One-Dimensional Modeling of Lower Hybrid Current Ramping in Tokamaks," in Proc. this meeting.

19. N. J. FISCH and C. F. F. KARNEY, Phys. Fluids, 24, 27 (1981).

20. W. A. HOULBERG, S. E. ATTENBERGER and L. L. LAO, "Developments in Tokamak Transport Modeling," Proc. Intnatl. Top. Meeting on Advances in Math. Methods for the Solution of Nucl. Eng. Problems, p. 426 (1981).

21. T. K. MAU, E. L. VOLD and R. W. CONN, "Fractional Power Operation of Tokamak Reactors: Issues and Prospects," PPG-964, UCLA (1986).

22. E. L. VOLD, T. K. MAU and R. W. CONN, "Ignition and Time-Dependent Fractional Power Operation of Tokamak Reactors," in Proc. this meeting.

23. S. M. KAYE, Phys. Fluids, 28, 2327 (1985).

24. M. KEILHACKER, "Confinement and Beta-Limit Studies in ASDEX H-Mode Discharges," in Proc. 10th Conf. on Plasma Physics and Controlled Nucl. Fusion Research, IAEA, London (1984).

25. P. J. BURNS, "TACO2D - A Finite Element Heat Transfer Code," UCID-17980, Lawrence Livermore Natl. Lab. (1982).

26. K. TAGHAVI and N. M. GHONIEM, "Primary Loop Conditioning and Design Constraints of Li-Pb Cooled Tandem Mirror Reactors During Start-up/Shutdown Operations," Nucl. Eng./Design Fusion, 1, 375 (1984).

27. BRÜNING, D. GUGGI and H. R. IHLE, "The Diffusivity of Tritium in the System Li_2O-Al_2O_3," in Proc. 12th Symp. on Fusion Technol., EUR 7983EN, pp. 543-548. (Julich, FRG, 1982).

28. R. G. CLEMMER et al., "The TRIO Experiment," ANL-84-55, Argonne Natl. Lab. (1984).

29. M. I. BASKES, "DIFFUSE-83," SAND-83-8231, Sandia Lab. (1983).